

pubs.acs.org/acsapm Article

Curing Characteristics of a Photopolymer Resin with Dispersed Glass Microspheres in Vat Polymerization 3D Printing

Jingyu Liang, Mathieu Francoeur, Christopher Bryant Williams, and Bart Raeymaekers*



Cite This: ACS Appl. Polym. Mater. 2023, 5, 9017-9026

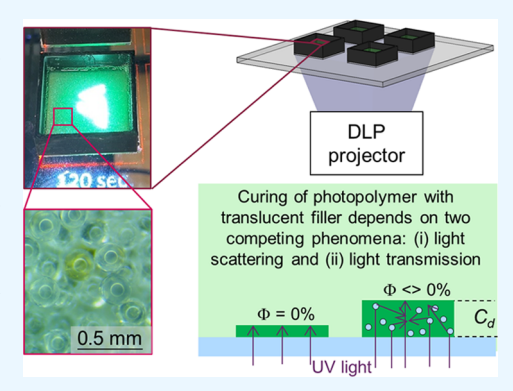


ACCESS I

Metrics & More

Article Recommendations

ABSTRACT: The curing characteristics of a photopolymer resin determine the relationship between the vat polymerization (VP) process parameters and the layer thickness, geometric accuracy, and surface roughness of the three-dimensional (3D) printed specimens. Dispersing a filler material into the photopolymer resin to modify the properties of the specimens changes the curing characteristics because the filler scatters, absorbs, and transmits light, which alters the photopolymerization reaction. However, the ability to cure the photopolymer resin with a high filler volume fraction is important to 3D print specimens for specific applications, such as composite and ceramic materials for biological and high-temperature environments. We specifically consider a translucent filler and methodically measure the curing characteristics of a diacrylate/epoxy photopolymer resin with dispersed translucent glass microspheres. Experiments relate the curing depth, degree-of-cure, geometric accuracy, and surface roughness to the exposure dose, filler fraction, and filler size



distribution. The curing depth depends on two competing effects: light scattering and light transmission through the translucent filler, and it increases with increasing filler fraction for low exposure dose, which contrasts results documented by others for VP with an opaque filler. Furthermore, the degree-of-cure increases with increasing filler fraction for a constant exposure dose. The geometric accuracy and surface roughness of the 3D printed specimens decrease with increasing exposure dose and filler fraction. This work has implications for VP of photopolymer resins with high filler fraction in the context of manufacturing of engineered materials.

KEYWORDS: vat polymerization, photopolymer, glass microspheres, degree-of-cure, curing depth

1. INTRODUCTION

Vat polymerization (VP) is a class of additive manufacturing (AM) processes that rely on selectively curing a photosensitive polymer (photopolymer) resin using visible or ultraviolet (UV) light in a layer-by-layer fashion to create a specimen with three-dimensional (3D) free-form geometry. A photopolymer resin typically comprises a mixture of monomers, oligomers, and photoinitiators, and exposure to light initiates cross-linking of polymer chains, which cures the liquid photopolymer resin into a solid material. The curing characteristics of the photopolymer resin determine the relationship between the VP process parameters and the layer thickness, geometric accuracy and resolution, and surface roughness of the 3D printed specimen.

Dispersing filler material in the photopolymer resin to modify the properties of the 3D printed specimen changes its curing characteristics. The filler scatters light, which affects the penetration depth of the light into the photopolymer resin, and it also increases the viscosity of the photopolymer, which modifies the polymerization reaction.^{3–6} However, the ability to increase the filler fraction dispersed in the photopolymer resin is important to 3D print material specimens for specific engineering applications, such as structural polymer matrix

composite materials where the filler provides strength and stiffness, 7-11 dental composite materials where the filler provides wear resistance, 12 electrical and thermal conductive polymer matrix composite materials where the filler creates a percolated network, 5,13-15 or polymer matrix composite materials with ceramic filler that, following resin pyrolysis particle sintering, finds use in biological and high-temperature environments. 16-18 Consequently, it is crucial to understand the curing characteristics of the photopolymer resin as a function of the filler fraction.

The curing characteristics of photopolymer are often quantified using the curing depth, which is the thickness of (a single layer of) the cured photopolymer specimen that results from a specific exposure dose, ^{3,4,19} and the degree-of-cure (DoC), which quantifies the ratio of the fully cured versus total photopolymer resin content of the specimen. ²⁰ Griffith

Received: July 4, 2023

Accepted: September 22, 2023 Published: October 11, 2023





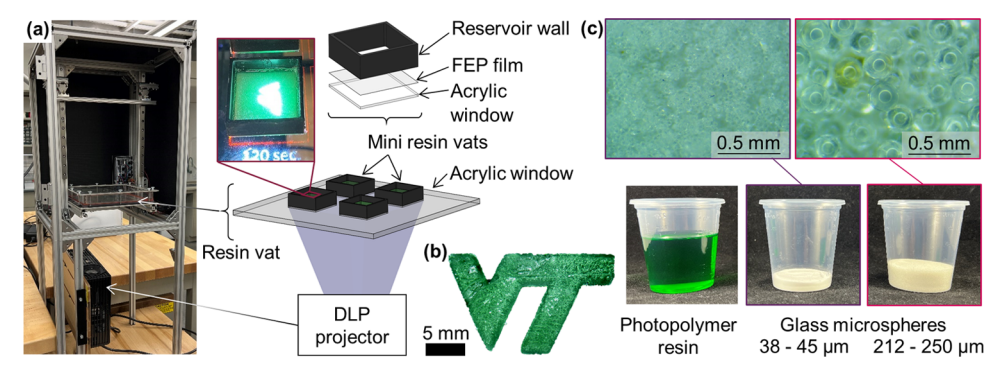


Figure 1. (a) Photo and schematic of the DLP VP platform, showing the setup with resin vat and acrylic window and several mini resin vats with acrylic window and FEP film, (b) a typical material specimen we 3D print in this work (Virginia Tech "VT" logo), and (c) translucent green photopolymer resin and glass microspheres.

and Halloran quantified the relationship between the light penetration depth, curing depth, and VP process parameters for an opaque ceramic filler dispersed in a photopolymer resin. They determined that light scattering increases with increasing filler fraction, which decreases light penetration depth into the photopolymer and, thus, decreases the curing depth. However, depending on the properties of the photopolymer resin and the filler, other researchers have shown that dispersing filler in the photopolymer resin can both increase (see, e.g., refs 21–23) and decrease (see, e.g., refs 23–25) the curing depth.

Several research groups have employed different methods to study the curing characteristics of photopolymer resins with dispersed filler materials: (i) using mechanical testing, in which photopolymer curing relates to the mechanical properties of the specimen; 21,24,26-28 (ii) using spectroscopy techniques such as Fourier transform infrared (FTIR)^{25,29-31} and Raman spectroscopy,³² which quantify the chemical composition and structure before and after curing; (iii) performing calorimetry measurements that relate the curing characteristics to heat generation during the exothermal curing reaction; 22,33-36 and (iv) implementing microscopy techniques that allow observing the material changes during the curing process. 25,29,37,38 Mechanical testing and thermal measurements average the curing measurement over the entire specimen, whereas Raman spectroscopy and microscopy average the curing measurement over a specific measurement location, which is typically substantially smaller than that of the specimen.

However, no studies methodically document and quantify the relationship between the curing characteristics and VP process parameters when using translucent instead of opaque filler material. Furthermore, no studies relate the geometric accuracy and surface topography of 3D printed specimens to the filler fraction and VP process parameters. Yet, this knowledge is crucial for VP of a photopolymer resin with a dispersed translucent filler, e.g., to manufacture engineered materials, and in particular, with high filler fraction or exposure dose, which is important to a myriad of high-performance, functional, engineered composite materials. Thus, the objective of this work is to experimentally determine the curing characteristics of a diacrylate/epoxy photopolymer resin with dispersed glass microspheres during VP. Specifically, we quantify and discuss the effect of filler fraction, filler size distribution, and exposure dose on the curing depth, degree-ofcure, geometric accuracy, and surface roughness of the 3D printed specimens.

2. METHODS AND MATERIALS

2.1. 3D Printing Specimens with VP. Figure 1a shows the opensource digital light processing (DLP) VP platform we used in this work (mUVe 3D, Grand Rapids, MI). The platform comprises a photopolymer resin vat with a 6 mm thick acrylic window that contains the photopolymer resin and a digital light projector (ViewSonic PJD7820HD, Brea, CA) equipped with a 210 W metal halide light source that projects visible and UV light (300-730 nm wavelength) to selectively cure the photopolymer resin.⁶ Additionally, mini photopolymer resin vats located within the main resin vat afford the ability to simultaneously cure multiple specimens with different filler fractions. The mini resin vats have a 1.5 mm thick acrylic window covered with a thin fluorinated ethylene propylene (FEP) film that provides chemical stability, and oxygen permeability gives it nonstick properties to release the cured photopolymer resin from the window.³⁹ We calibrate the projector to focus within the plane of the FEP film of the mini resin vats to ensure maximum accuracy of the 3D printed specimens, and we verify that each mini resin vat receives an identical exposure dose from the light source.

Figure 1b illustrates the geometry of the 3D printed material specimens, i.e., the Virginia Tech VT logo, which contains internal and external features, straight lines, and sharp corners and, thus, allows a qualitative and quantitative assessment of the geometry after curing, as a function of the filler fraction and VP process parameters. We use a consumer-grade photopolymer resin specifically formulated for DLP VP with density $\rho=1.05-1.25~{\rm g/cm^3}$ (Anycubic standard UV resin translucent green, Anycubic 3D Inc., Shenzhen, China) (see Figure 1c). It is a mixed cationic/radical photopolymer that consists of 60% epoxy resin, 35% tripropylene glycol diacrylate ($C_{15}H_{24}O_6$), 5% hydroxycyclohexyl phenyl ketone ($C_{13}H_{16}O_2$), and sulfonium salt. Epoxy resin and tripropylene glycol diacrylate are cationic and free radical monomers that cross-link during the curing process, initiated by the sulfonium salt (cationic) and hydroxycyclohexyl phenyl ketone (radical) photoinitiator.

We select glass microspheres as filler material, with bulk density of 1.5-1.6 g/cm³, specific gravity of 2.5-2.6 g/cm³, and refractive index of 1.50–1.52, and we use two different size distributions: $38-45 \mu m$ (small) and 212–250 μm (large) diameter (Novum Glass LLC, Rolla, MO) (see Figure 1c).⁴¹ The glass microspheres are translucent, and we experimentally verified high transmission and low absorption within the visible and UV light bandwidth. We disperse the filler in the photopolymer resin using shear mixing with a magnetic stirrer and use mixtures with filler weight fractions $\Phi_{\rm m}$ = 0, 15, 30, 45, and 60 wt %, which corresponds to filler volume fractions $\Phi = 0$, 8, 16, 27, and 41 vol % (using specific gravity). Additionally, we consider monodisperse mixtures of the photopolymer resin that contain a single glass microsphere size distribution (small or large) and polydisperse mixtures with half (by volume) of both small and large microsphere size distributions. Virgin photopolymer resin with Φ_m = $\Phi = 0$ serves as a benchmark throughout this work.

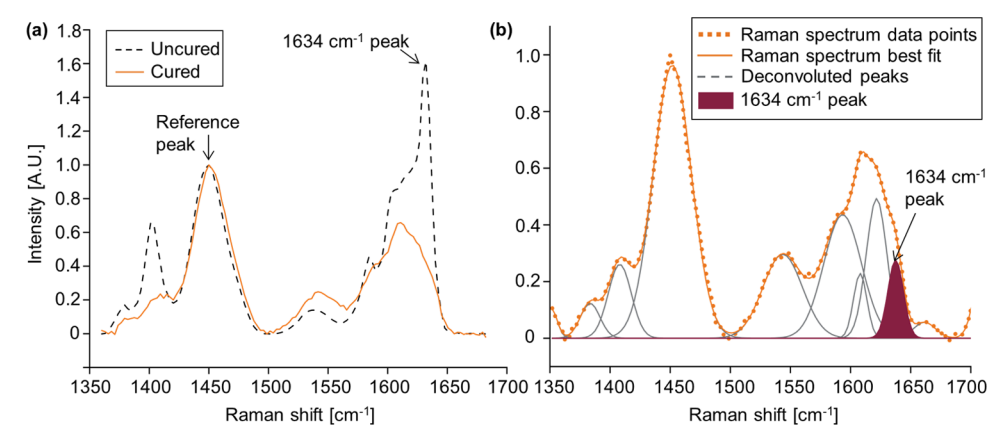


Figure 2. (a) Comparison between the Raman spectra of an uncured (black dashed line) and cured (orange solid line) photopolymer specimen (baseline adjusted and normalized with the reference peak that is invariant to the degree-of-cure), showing the 1634 cm⁻¹ peak that represents C= C bonds, which decreases with increasing degree-of-cure. (b) Typical Raman spectroscopy data (orange dots) with best fit (orange solid line) and deconvoluted peaks (gray solid lines) using a Gaussian best fit. Comparing the area of the deconvoluted 1634 cm⁻¹ peak between specimens allows quantification of the degree-of-cure.

We measure the light intensity I inside the acrylic window of the mini resin vats using a UV light meter (Lingshang LLC LS126A, Shenzhen, China), to determine the exposure dose E_0 = It, where t is the curing time. The exposure dose quantifies the amount of light energy incident to the photopolymer resin during curing. In this VP setup, each mini resin vat receives the same incident light intensity, I = 12 mW/cm², which remains constant for all experiments in this work. Thus, we change the exposure dose E_0 using different curing times of t = 5, 10, 15, 20, 30, 60, 120, and 180 s, which correspond to $E_0 = 60$, 120, 180, 240, 360, 720, 1440, and 2160 mJ/cm². The choice of curing times t and corresponding exposure doses E_0 allows monitoring photopolymer resin curing within short (5 s) time intervals during the first 20 s when the resin cures fast, and within large (>10 s) time intervals after the first 20 s, when curing slows down because solid, cured photopolymer with the filler increasingly inhibits light from penetrating in the remaining liquid photopolymer resin. We note that we include exposure dose values in this work that are substantially larger than those typically used in commercial VP processes to understand the curing characteristics of the photopolymer resin, even under extreme conditions. Correspondingly, the curing depth for high exposure dose values is larger than what one would typically measure for a single material layer during VP. We perform a full-factorial study of filler volume fraction Φ (five treatment levels), filler size distribution (three treatment levels: small, large, 50/50 mix), and exposure dose E_0 (eight treatment levels) to systematically determine the effect of these VP process parameters and their potential interaction effects on the curing characteristics of the photopolymer resin. Since we use three replications of each experiment, we manufacture a total of 8×3 ($\Phi = 0\%$) + $4 \times 3 \times 8 \times 3$ $(\Phi > 0\%) = 312$ specimens (see Figure 1b).

2.2. Specimen Characterization. We measure the curing depth $C_{\rm d}$ of each specimen at four locations along the geometry of the VT specimen using digital calipers, and we calculate the average thickness of the four measurements. Calipers are inexpensive, fast, and reliable, even though more sophisticated methods have recently become available. The curing depth $C_{\rm d}$ relates to the light penetration depth $D_{\rm p}$, the exposure dose $E_{\rm o}$, and the critical exposure dose $E_{\rm c}$, which is the minimum energy to initiate curing, as described by the Beer–Lambert law, 19,43 i.e.,

$$C_{\rm d} = D_{\rm p} \ln \left(\frac{E_0}{E_{\rm c}} \right) \tag{1}$$

When light penetrates a medium, its intensity exponentially decreases with increasing penetration depth. 43,44 Thus, the relationship between the curing depth C_d and the exposure dose E_0 is usually presented as a semilogarithmic plot and referred to as the "working curve" of the

photopolymer resin. 45,46 The slope of a logarithmic curve fit of experimental working curve data represents the penetration depth $D_{\rm p}$, whereas the intercept with the exposure dose axis indicates the critical exposure dose $E_{\rm c}$.

We also use Raman spectroscopy (Horiba XploRA Plus, Horiba Instruments Inc., Irvine, CA) to determine the degree-of-cure of all specimens, which describes the fraction of cross-linked polymer chains within the photopolymer resin between 0 (uncured) and 1 (fully cured). Prior to analysis, we normalize and adjust the baseline of all Raman spectra with respect to a reference peak (Raman shift of 1455 cm⁻¹), which represents stable CH₂ bonds that do not participate in the photopolymerization reaction and, thus, remains invariant to the degree-of-cure of the epoxy/diacrylate mixture.²⁰ During the polymerization reaction, the double C=C bonds in the diacrylate monomers break into single bonds and cross-link with other monomers. Figure 2a shows typical Raman spectra of an uncured liquid photopolymer resin (black dashed line) and a solid photopolymer resin specimen cured with an $E_0 = 2160 \text{ mJ/cm}^2$ (orange solid line). We indicate the reference peak (1455 cm⁻¹) and, additionally, we observe that the 1634 cm⁻¹ peak (C=C bonds) decreases with increasing degree-of-cure (black dashed line compared to orange solid line). However, determining the magnitude of the 1634 cm⁻¹ peak in the Raman spectrum is not straightforward because multiple peaks overlap and, thus, they must first be deconvoluted. Figure 2b shows the Raman spectroscopy measurement data of a typical cured photopolymer resin specimen (orange dots) with a curve fit through the data points to obtain the Raman spectrum best fit (orange line). The deconvolution of the Raman spectrum is based on a Gaussian best fit to individual peaks (gray solid lines).⁴⁷ We indicate the area of the 1634 cm⁻¹ peak (maroon), isolated from other adjacent peaks that may be due to noise from, e.g., fluorescence, contamination, and other compounds in the photopolymer resin. Thus, comparing the area of the 1634 cm⁻¹ peak (maroon) between different specimens allows quantifying the degree-of-cure (DoC) as 48

$$DoC = 1 - \frac{A_{1634}(t)}{A_{1634}(0)} \tag{2}$$

where $A_{1634}(t)$ and $A_{1634}(0)$ are the area of the 1634 cm⁻¹ peak after curing time t and at time t = 0 (uncured), respectively.

We quantitatively compare the geometry of the 3D printed specimens to the computer-aided design (CAD) drawing of the specimen geometry using an optical microscope (AMSCOPE, Irvine, CA), and we measure the specimen in the x- and y-direction to quantify the so-called "profile broadening" or "overcuring", i.e., cured photopolymer resin in excess of the intended specimen geometry as defined in the CAD drawing. We also measure the surface topography of the 3D printed specimen using a laser optical profilometer with

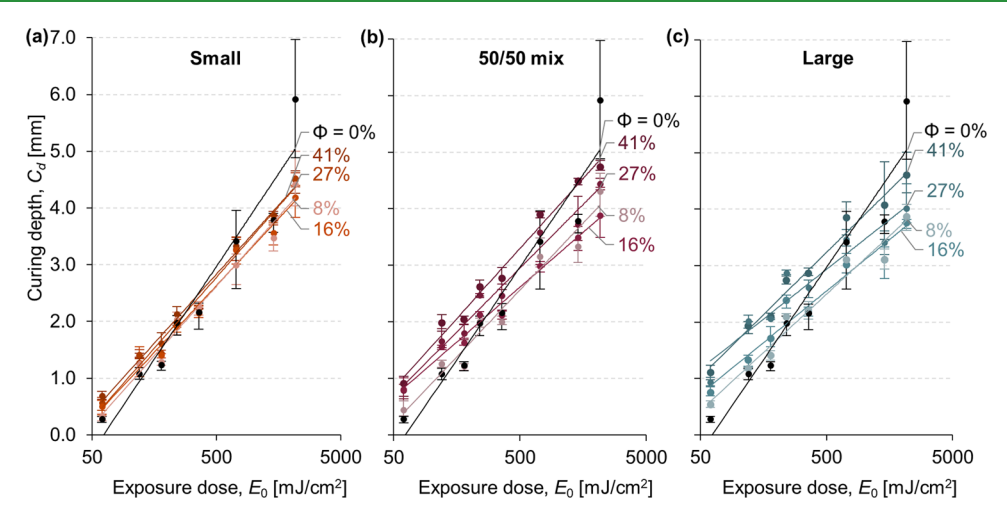


Figure 3. Photopolymer working curves, showing curing depth C_d versus exposure dose E_0 (semilogarithmic), for different filler volume fractions Φ (color gradient) and for different filler size distributions (color): (a) small, (b) 50/50 mix, and (c) large. Each data point represents the average of three measurements, and the error bars show the minimum and maximum values.

optical focus variation mode to avoid laser scattering at the surface when using laser confocal mode (Keyence VK-X3000, Raleigh, NC). Specifically, we determine the surface topography of the 3D printed specimen surface furthest away from the resin vat window, which represents a measure of the 3D printing quality. We correct the surface topography measurements for specimen tilt, and we shift the center plane of all surface heights to zero prior to determining the mean surface roughness *Sa* over the entire 5 mm by 4 mm field-ofview of the measurement.⁴⁹

3. RESULTS AND DISCUSSION

3.1. Curing Depth. Figure 3 shows the curing depth C_d versus the exposure dose E_0 (semilogarithmic plot, the socalled working curve) for different filler volume fractions Φ and for different filler size distributions: (a) small, (b) 50/50 mix, and (c) large. The solid black line shows virgin photopolymer resin ($\Phi = 0\%$). Each data point represents the average of three measurements, and the error bars show the minimum and maximum values. We add a logarithmic best fit of the experimental data for each filler volume fraction Φ to visualize the slope of the working curve, which represents the light penetration depth D_p (see eq 1). For the virgin photopolymer, we quantify $E_c = 61.7 \text{ mW/cm}^2$ and $D_p =$ 1.42 mm. From Figure 3, we observe that the curing depth increases with increasing exposure dose, independent of the filler volume fraction and the filler size distribution because the energy incident to the photopolymer increases. However, the incremental increase of curing depth decreases with increasing exposure dose, as expected from the Beer-Lambert law (see eq 1) because the light intensity attenuates exponentially with increasing light penetration depth in the photopolymer. 45 We also observe that the light penetration depth D_p (slope of the working curve) decreases slightly with increasing filler volume fraction. Additionally, comparing Figure 3a—c, we observe that the critical exposure dose E_c (intercept with the exposure dose axis) decreases with both increasing filler volume fraction for constant filler size distribution and with increasing filler size distribution for constant filler volume fraction.

The results suggest that the curing characteristics of the photopolymer resin with a dispersed translucent filler (glass microparticles) are driven by two competing phenomena: (i) light scattering, which redirects light that interacts with the filler into the photopolymer resin and, thus, increases light

intensity attenuation with increasing penetration depth, and (ii) light transmission through the translucent filler in the photopolymer, which cures the photopolymer behind the filler. Light scattering increases with increasing filler volume fraction, and the intensity of the scattered light increases with increasing filler size distribution, ⁵⁰ which both increase the scattered light that redirects into the photopolymer resin and, consequently, lowers the threshold to initiate the curing reaction $E_{\rm c}$. Light transmission through the translucent filler decreases with decreasing filler size distribution for a constant filler volume fraction, which we verified experimentally with light intensity measurements.

Thus, based on these two competing phenomena, the light penetration depth D_p decreases when dispersing the filler in the photopolymer, and consequently, the working curves of the photopolymer with dispersed filler ($\Phi \neq 0\%$) show a shallower slope than that of the virgin photopolymer resin ($\Phi = 0\%$). Furthermore, increasing the filler volume fraction (within the range we evaluate) increases light scattering, but it also increases light transmission through the translucent filler in the photopolymer resin. Figure 3 shows that both effects appear to balance each other, as the slope of the working curves is almost independent of the filler volume fraction for a constant filler size distribution. In contrast, the slope of the working curve decreases with increasing filler size distribution because light scattering (decreases light penetration) dominates light transmission (increases light penetration), as the intensity of the scattered light increases with increasing filler size. 50

These results are in agreement with those published by Martin et al.²⁰ and Choong et al.²¹ However, they contrast the results presented by, e.g., Xu et al.,²⁹ who used opaque instead of translucent filler material, and documented that the curing depth decreases with increasing filler fraction. When using opaque instead of translucent filler material, the curing characteristics also depend on light absorption, i.e., the filler scatters and absorbs light but does not transmit it through the filler. Hence, an opaque filler blocks light to the photopolymer behind it, whereas a translucent filler allows light to pass through and cure the photopolymer, which explains the different results. The opacity of the filler and its refractive index determine the fraction of incident light that passes through.

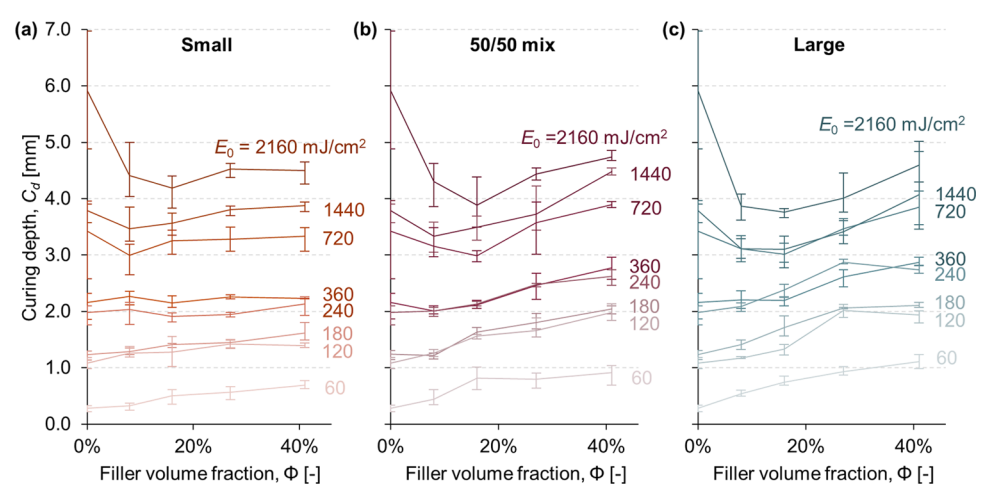


Figure 4. Curing depth C_d versus filler volume fraction Φ (color gradient), for different values of the exposure dose E_0 and for different filler size distributions (color): (a) small, (b) 50/50 mix, and (c) large. Each data point represents the average of three measurements, and the error bars show the minimum and maximum values.

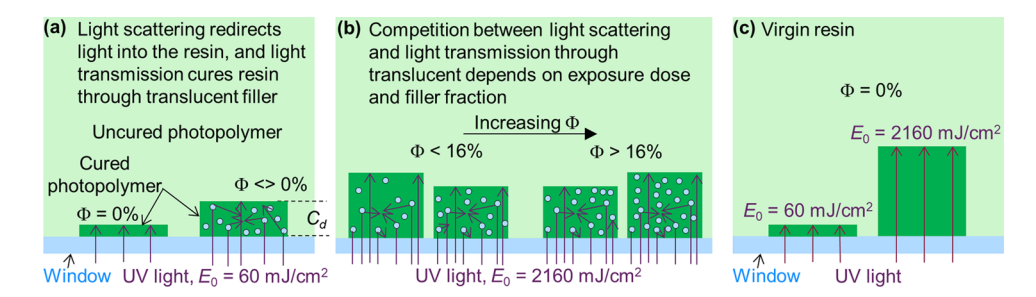


Figure 5. Schematic representation of light scattering and transmission, showing (a) light scattering from the filler redirects within the photopolymer resin and light transmits through the translucent filler to cure the photopolymer behind it, thus increasing the curing depth for constant exposure dose, (b) competition between light scattering and light transmission depends on the exposure dose and the filler volume fraction, and (c) maximum curing depth occurs for the virgin photopolymer and maximum exposure dose.

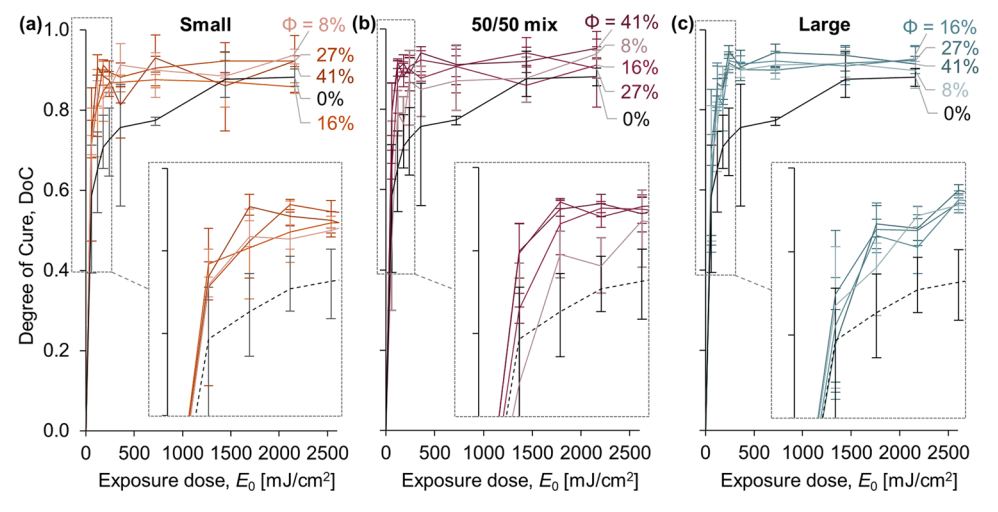


Figure 6. Degree-of-cure (DoC) versus exposure dose E_0 , for different filler volume fractions Φ (color gradient) and for different filler size distributions (color): (a) small, (b) 50/50 mix, and (c) large. Each data point represents the average of three measurements, and the error bars show the minimum and maximum values.

Figure 4 shows the curing depth $C_{\rm d}$ versus the filler volume fraction Φ for different values of the exposure dose $E_{\rm 0}$ and for different filler size distributions: (a) small, (b) 50/50 mix, and (c) large. Each data point represents the average of three measurements, and the error bars show the minimum and maximum values. The data of Figure 4 are identical to that of Figure 3 and also illustrate that the curing depth increases with

increasing exposure dose and with increasing filler size distribution. However, Figure 4 reveals additional aspects of the curing characteristics of the photopolymer resin with a dispersed filler compared to Figure 3. Specifically, we observe from Figure 4 that when $E_0 < 360 \text{ mJ/cm}^2$, the curing depth increases with increasing filler volume fraction, which agrees with results documented by Schlotthauer et al.²³ However,

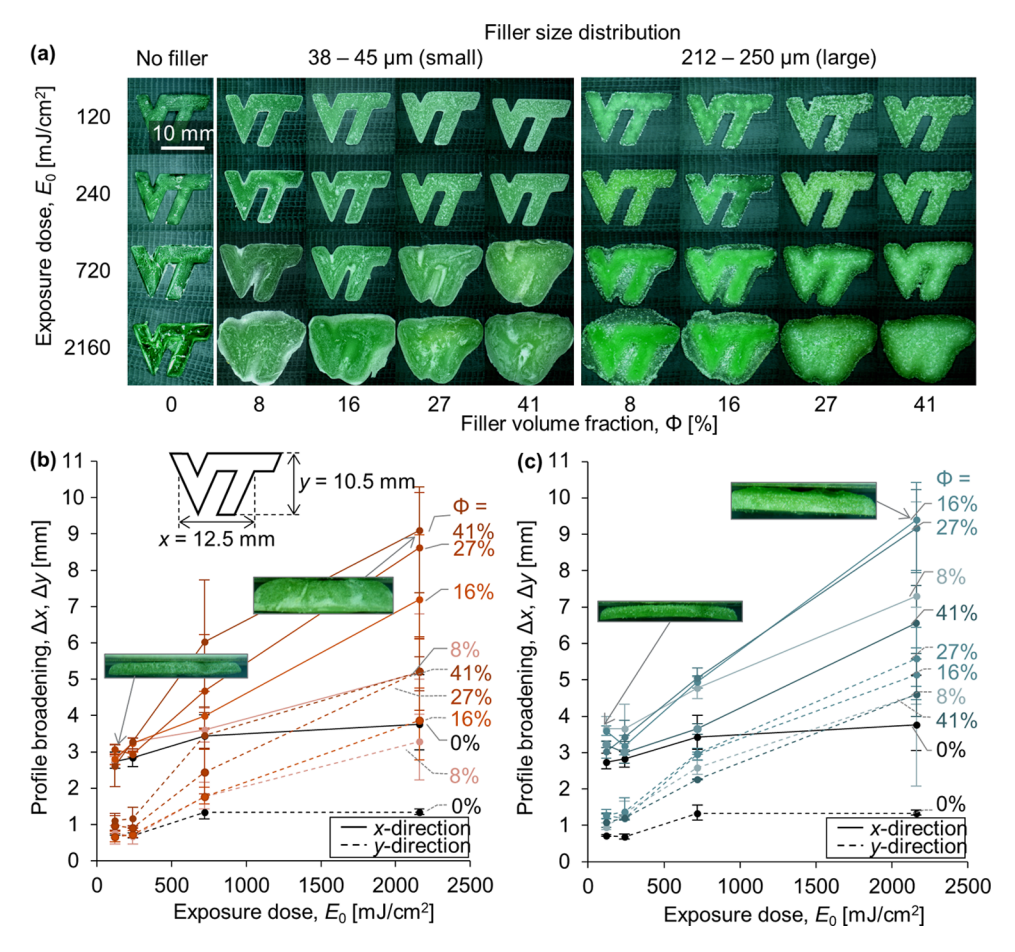


Figure 7. Profile broadening of the 3D printed VT logo specimens for different combinations of exposure dose E_0 and filler volume fraction Φ (color gradient), and for two different filler size distributions: small (left) and large (right), showing (a) a selection of optical images of the specimens, qualitatively illustrating profile broadening, and Δx - (solid lines) and Δy - (dashed lines) measurement (with respect to the CAD drawing in the inset image) for filler size distribution: (b) small and (c) large. Additional inset images show side (profile) views of the 3D printed specimens.

when $E_0 > 720$ mJ/cm², the curing depth first decreases and then increases with an increasing filler volume fraction. We explain these results by considering the competition between light scattering and light transmission through the translucent filler.

Figure 5 schematically illustrates the relationship between light scattering, light transmission through the translucent filler, exposure dose, and filler volume fraction, as informed by the experimental results of Figures 3 and 4. The filler scatters the incident light, redirects it within the photopolymer resin and, thus, lowers the critical exposure dose to initiate the polymerization reaction. Simultaneously, light transmits through the translucent filler and cures the photopolymer behind it, which increases the curing depth for constant exposure dose (Figure 5a). However, the light intensity also attenuates with increasing filler volume fraction due to scattering. Thus, when the filler volume fraction Φ < 16% (and $E_0 > 720$ mJ/cm²), the curing depth decreases with increasing filler volume fraction for constant exposure dose because light intensity attenuation due to scattering dominates over light transmission through the translucent filler (Figure 5b). However, for $\Phi > 16\%$ (and $E_0 > 720$ mJ/cm²), the curing depth increases with increasing filler volume fraction for constant exposure dose because light transmission through the translucent filler dominates over light intensity attenuation due to scattering (Figure 5b). Since 720 mJ/cm² is substantially larger than the exposure dose typically used in commercial VP processes, the practical importance of curing characteristics with high exposure doses in the context of common engineering applications may be limited. Also note that the curing depth is maximum when $\Phi=0\%$ in combination with the maximum exposure dose because the light penetration depth is maximum when $\Phi=0\%$, resulting from the steepest working curve (Figure 5c).

3.2. Degree-of-Cure. Figure 6 shows the degree-of-cure versus the exposure dose E_0 for different filler volume fractions Φ and for different filler size distributions: (a) small, (b) 50/50 mix, and (c) large. The solid black line represents the virgin photopolymer resin ($\Phi = 0\%$). Each data point represents the average of three measurements, and the error bars show the minimum and maximum values. We show magnified inset images for E_0 < 250 mJ/cm². From Figure 6, we observe that the degree-of-cure increases with increasing exposure dose, independent of the filler volume fraction and filler size distribution. Furthermore, we observe that any combination of filler volume fraction and filler size distribution approaches a 90% degree-of-cure with increasing exposure dose, which agrees with the results documented by Jiang and Drummer.⁵¹ The filler scatters incident light, redirects it within the photopolymer resin and, thus, lowers the critical exposure dose for the photopolymer curing reaction. Hence, it explains that the degree-of-cure of the photopolymer resin with any

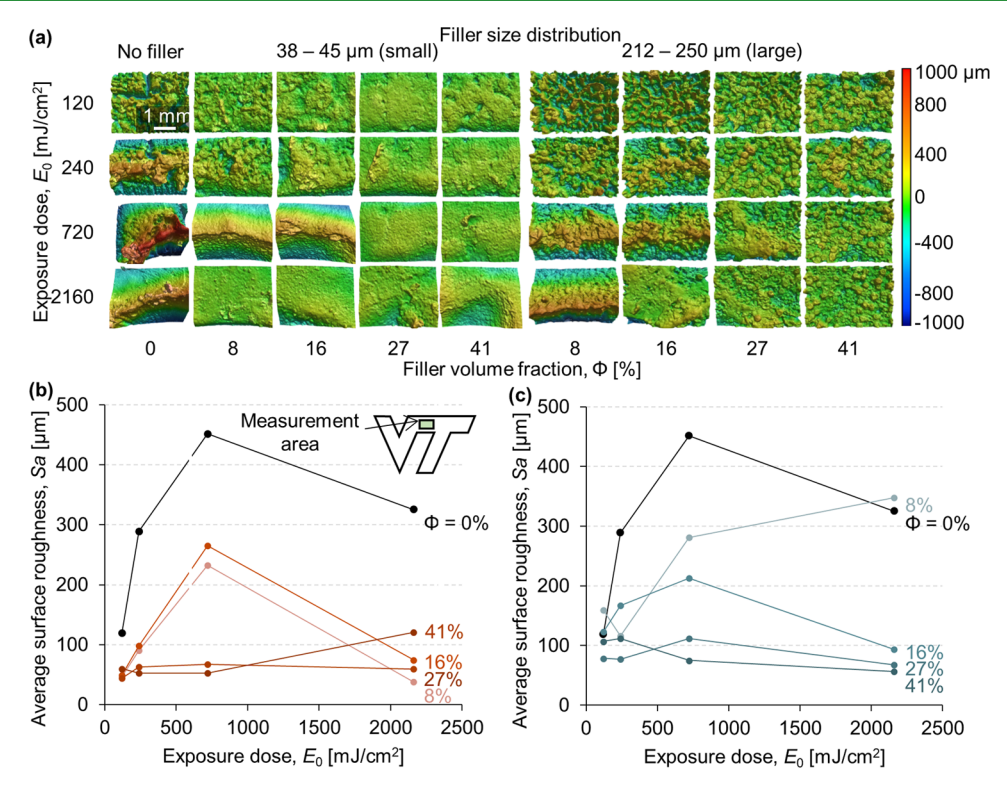


Figure 8. Surface topography of the surface of the 3D printed specimen furthest away from the resin vat window for different combinations of exposure dose E_0 and filler volume fraction Φ (color gradient), and for two different filler size distributions: small (left) and large (right), showing (a) surface topography maps, and the average surface roughness Sa for (b) small, and (c) large filler size distribution.

filler ($\Phi \neq 0\%$) exceeds that of the virgin photopolymer resin ($\Phi = 0\%$), independent of exposure dose and filler size distribution. The degree-of-cure also appears to increase with increasing filler volume fraction and increasing filler size distribution, which agrees with the results of Figure 4. However, the error bars overlap in Figure 6, which prevents a conclusive assessment.

3.3. Geometric Accuracy. Figure 7a shows a selection of optical images of 3D printed VT logo specimens for different combinations of exposure dose E_0 (rows) and filler volume fraction Φ (columns) and for different filler size distributions: small (left) and large (right). From Figure 7a, we qualitatively observe that the geometric accuracy of the 3D printed specimens decreases with increasing exposure dose, which is known as profile broadening or overcuring, and is caused by light scattering from the filler as well as cured contours of the 3D printed specimen.²³ Thus, the importance of profile broadening increases with increasing filler volume fraction and increasing exposure dose, which is evident from Figure 7a. For instance, comparing a specimen with $E_0 = 720 \text{ mJ/cm}^2$ and Φ = 27% to one with E_0 = 720 mJ/cm² and Φ = 41% displays more profile broadening for the latter than the former. In contrast, the equivalent specimens with $E_0 = 240 \text{ mJ/cm}^2 \text{ show}$ almost no profile broadening. An exposure dose of E_0 = 2160 mJ/cm² causes complete loss of shape for all specimens independent of the filler volume fraction. Profile broadening also increases with increasing filler size distribution because the effect of light scattering increases with increasing particle size, independent of the exposure dose and filler volume fraction.⁵

Figure 7b, c quantify profile broadening of the specimens of Figure 7a by determining the difference Δx and Δy between a measurement in the x- and y-direction to the corresponding dimensions of the CAD drawing of the specimen (see inset

image of Figure 7b), as a function of exposure dose E_0 , and for different values of the filler volume fraction Φ , and for both the small (Figure 7b) and large (Figure 7c) filler size distribution. The solid and dashed lines represent profile broadening in the x- and y-direction, respectively. The line colors refer to different filler volume fractions ($\Phi \neq 0\%$), whereas the black lines represent virgin photopolymer ($\Phi = 0\%$). Each data point is the average of three measurements, and the error bars show the minimum and maximum values. From Figure 7b,c, we observe that profile broadening increases with increasing exposure dose and increasing filler volume fraction for both the x- and y-measurements. We also observe a slight increase of profile broadening for the large versus the small filler size distribution because the intensity of the scattered light increases with increasing filler size distribution. Side views of selected specimens (inset images in Figure 7b,c) demonstrate that profile broadening decreases with increasing penetration depth (build direction) and is most pronounced closest to the window, where the light intensity is maximum. The virgin photopolymer ($\Phi = 0\%$) displays minimal profile broadening because the absence of filler material reduces sources of light scattering to the cured contours of the specimen only.

3.4. Surface Topography. Figure 8a shows the surface topography maps of the surface furthest away from the curing window (within the center portion between the letters V and T in the VT logo, see inset of Figure 8b), using a color scale to represent the surface height z at each x- and y-coordinate within the measurement area, i.e., z = f(x,y). We observe that the surface topography of virgin photopolymer specimens ($\Phi = 0\%$) is spiky compared to that of specimens with a dispersed filler ($\Phi \neq 0\%$) because, in the absence of the filler, the incident UV light penetrates the virgin photopolymer resin without interacting with the filler (see also Figures 3 and 4).

Additionally, we observe that the surface topography features match the size of the filler size distribution, which is easiest to recognize for the surface topography maps of the specimens with large filler size distribution. When $0 < \Phi < 8\%$, the surface topography is mostly dominated by the cured photopolymer, when 8 < Φ < 21%, a combination of resin and filler determines the surface topography, but when $\Phi > 21\%$, the surface topography almost entirely comprises filler material.

Figure 8 shows the average surface roughness Sa versus the exposure dose E_0 for different values of filler volume fraction Φ, and for different filler size distributions: (a) small and (b) large. The black line represents the virgin photopolymer resin $(\Phi = 0\%)$. We observe the highest Sa values for the virgin photopolymer resin specimens ($\Phi = 0\%$), which results from the spiky topography at the center of the surface and measurement domain. The center shows a greater curing depth compared to its surroundings, which we observe as "ridge"-type topography features in some of the subfigures of Figure 8a, e.g., $E_0 = 2160 \text{ mJ/cm}^2$ and $\Phi = 0\%$. These features result from a convex lens-shaped layer that forms during photopolymer curing and focuses the incoming light into the center. It is sometimes referred to as superlogarithmic behavior, and it is driven by photobleaching and self-

Furthermore, the average surface roughness decreases with increasing filler volume fraction because the close-packing of filler material in combination with light scattering creates a smooth surface. We note that specimens that show substantial profile broadening, which increases with increasing filler volume fraction, also display a smooth surface topography. Conversely, we observe from Figure 8b,c that the average surface roughness first increases and then decreases with increasing exposure dose, due to the interplay between light scattering, filler volume fraction, and light transmission through the translucent filler. Finally, we observe that the average surface roughness Sa increases slightly with increasing filler size distribution, in particular for specimens cured with low exposure dose (E_0 < 240 mJ/cm²), even though a clear pattern does not emerge from the results.

4. CONCLUSIONS

We experimentally determine the curing characteristics of a diacrylate/epoxy photopolymer resin with dispersed glass microspheres. Specifically, we quantify the effect of exposure dose E_0 , filler volume fraction Φ , and filler size distribution on the degree-of-cure and the curing depth C_d during the DLP VP process. We also evaluated the geometric accuracy of the 3D printed specimens and measured their surface roughness. We conclude that

(1) The curing characteristics of a photopolymer resin with a dispersed translucent filler (glass microparticles) depend on two competing phenomena: (i) light scattering, which redirects light that interacts with the filler into the photopolymer resin and, thus, increases light intensity attenuation with increasing penetration depth, and (ii) light transmission through the translucent filler in the photopolymer, which cures the photopolymer behind the filler. Light scattering increases with increasing filler volume fraction, and the intensity of the scattered light increases with increasing filler size distribution, both increasing the scattered light that redirects into the photopolymer resin and,

consequently, lowers the threshold to initiate the curing reaction E_c . However, light transmission through the translucent filler decreases with decreasing filler size distribution for constant filler volume fraction, which we verified experimentally with light intensity measure-

- (2) The curing depth C_d depends on both the exposure dose E_0 and the filler volume fraction Φ . Both light scattering and light transmission through the filler increase with increasing filler volume fraction. When the exposure dose E_0 < 360 mJ/cm², light transmission through the translucent filler dominates over light scattering, and the curing depth increases with increasing exposure dose, filler volume fraction, and filler size distribution. In contrast, when the exposure dose $E_0 > 720 \text{ mJ/cm}^2$, light scattering dominates over light transmission for small filler volume fraction (Φ < 16%), which decreases the curing depth with increasing filler volume fraction, and transmission dominates over light scattering for large filler volume fraction ($\Phi > 16\%$), which increases the curing depth with increasing filler volume fraction.
- (3) The degree-of-cure DoC increases with increasing exposure dose E_0 and increasing filler volume fraction Φ but ultimately approaches 90% with increasing exposure dose. The addition of filler $(\Phi \neq 0\%)$ decreases the slope of the photopolymer working curve compared to the virgin photopolymer resin (Φ = 0%) and, thus, decreases the critical exposure dose, i.e., the addition of filler lowers the threshold to initiate the curing reaction because light scattering redirects light back into the photopolymer.
- (4) The geometric accuracy of the 3D printed specimens decreases with increasing exposure dose and with increasing filler volume fraction because light that scatters from filler and the contours of the 3D printed specimens induces undesirable curing.
- (5) The average surface roughness Sa of the 3D printed specimens first increases and then decreases with increasing exposure dose E_0 , and it decreases with increasing filler volume fraction Φ , due to interplay between filler volume fraction, light scattering, and light intensity attenuation.

AUTHOR INFORMATION

Corresponding Author

Bart Raeymaekers - Department of Mechanical Engineering, Virginia Tech, Blacksburg, Virginia 24061, United States; orcid.org/0000-0001-5902-3782;

Email: bart.raeymaekers@vt.edu

Authors

Jingyu Liang - Department of Mechanical Engineering, Virginia Tech, Blacksburg, Virginia 24061, United States Mathieu Francoeur — Department of Mechanical Engineering, McGill University, Montréal, QC H3A 0C3, Canada; orcid.org/0000-0003-4989-4861

Christopher Bryant Williams – Department of Mechanical Engineering, Virginia Tech, Blacksburg, Virginia 24061, United States; orcid.org/0000-0002-0499-2444

Complete contact information is available at: https://pubs.acs.org/10.1021/acsapm.3c01479

Notes

The authors declare no competing financial interest.

ACKNOWLEDGMENTS

Note that portions of this work are part of the Master of Science thesis of J.L. B.R., J.L., and M.F. acknowledge support from the National Science Foundation under award CMMI-2130083. Additionally, this work was made possible by the use of Virginia Tech's Materials Characterization Facility, which is supported by the Institute for Critical Technology and Applied Science, the Macromolecules Innovation Institute, and the Office of the Vice President for Research and Innovation. The VT logo contained herein is a registered trademark of Virginia Polytechnic Institute and State University (Virginia Tech).

REFERENCES

- (1) Gibson, I.; Rosen, D.; Stucker, B. Additive Manufacturing Technologies: 3D Printing, Rapid Prototyping, and Direct Digital Manufacturing; Springer: New York, NY, 2015. DOI: 10.1007/978-1-4939-2113-3.
- (2) Bagheri, A.; Jin, J. Photopolymerization in 3D Printing. ACS Appl. Polym. Mater. 2019, 1 (4), 593–611.
- (3) Griffith, M. L.; Halloran, J. W. Freeform Fabrication of Ceramics via Stereolithography. J. Am. Ceram. Soc. 2005, 79 (10), 2601–2608.
- (4) Chartier, T.; Chaput, C.; Doreau, F.; Loiseau, M. Stereolithography of Structural Complex Ceramic Parts. *J. Mater. Sci.* **2002**, 37 (15), 3141–3147.
- (5) Niendorf, K.; Raeymaekers, B. Combining Ultrasound Directed Self-Assembly and Stereolithography to Fabricate Engineered Polymer Matrix Composite Materials with Anisotropic Electrical Conductivity. *Composites, Part B* **2021**, 223, No. 109096.
- (6) Greenhall, J.; Raeymaekers, B. 3D Printing Macroscale Engineered Materials Using Ultrasound Directed Self-Assembly and Stereolithography. *Adv. Mater. Technol.* **2017**, 2 (9), No. 1700122.
- (7) Thostenson, E. T.; Chou, T.-W. Aligned Multi-Walled Carbon Nanotube-Reinforced Composites: Processing and Mechanical Characterization. J. Phys. D: Appl. Phys. 2002, 35 (16), L77–L80.
- (8) Haslam, M. D.; Raeymaekers, B. Aligning Carbon Nanotubes Using Bulk Acoustic Waves to Reinforce Polymer Composites. *Composites, Part B* **2014**, *60*, 91–97.
- (9) Scholz, M.-S.; Drinkwater, B. W.; Trask, R. S. Ultrasonic Assembly of Anisotropic Short Fibre Reinforced Composites. *Ultrasonics* **2014**, *54* (4), 1015–1019.
- (10) Greenhall, J.; Homel, L.; Raeymaekers, B. Ultrasound Directed Self-Assembly Processing of Nanocomposite Materials with Ultra-High Carbon Nanotube Weight Fraction. *J. Compos. Mater.* **2019**, 53 (10), 1329–1336.
- (11) Felt, A.; Raeymaekers, B. Ultrasound Directed Self-Assembly of Filler in Continuous Flow of a Viscous Medium through an Extruder Nozzle for Additive Manufacturing. *Addit. Manuf. Lett.* **2023**, *S*, No. 100120.
- (12) Tanimoto, Y.; Hayakawa, T.; Nemoto, K. Analysis of Photopolymerization Behavior of UDMA/TEGDMA Resin Mixture and Its Composite by Differential Scanning Calorimetry. *J. Biomed. Mater. Res., Part B* **2005**, 72 (2), 310–315.
- (13) Melchert, D. S.; Collino, R. R.; Ray, T. R.; Dolinski, N. D.; Friedrich, L.; Begley, M. R.; Gianola, D. S. Flexible Conductive Composites with Programmed Electrical Anisotropy Using Acoustophoresis. *Adv. Mater. Technol.* **2019**, *4* (12), No. 1900586.
- (14) Niendorf, K.; Raeymaekers, B. Quantifying Macro- and Microscale Alignment of Carbon Microfibers in Polymer-Matrix Composite Materials Fabricated Using Ultrasound Directed Self-Assembly and 3D-Printing. *Composites, Part A* **2020**, *129*, No. 105713.
- (15) Niendorf, K.; Raeymaekers, B. Using Supervised Machine Learning Methods to Predict Microfiber Alignment and Electrical Conductivity of Polymer Matrix Composite Materials Fabricated with

- Ultrasound Directed Self-Assembly and Stereolithography. Comput. Mater. Sci. 2022, 206, No. 111233.
- (16) Kalsoom, U.; Peristyy, A.; N Nesterenko, P.; Paull, B. A 3D Printable Diamond Polymer Composite: A Novel Material for Fabrication of Low Cost Thermally Conducting Devices. *RSC Adv.* **2016**, *6* (44), 38140–38147.
- (17) Ferrage, L.; Bertrand, G.; Lenormand, P.; Grossin, D.; Ben-Nissan, B. A Review of the Additive Manufacturing (3DP) of Bioceramics: Alumina, Zirconia (PSZ) and Hydroxyapatite. *J. Aust. Ceram. Soc.* **2017**, 53 (1), 11–20.
- (18) Zakeri, S.; Vippola, M.; Levänen, E. A Comprehensive Review of the Photopolymerization of Ceramic Resins Used in Stereo-lithography. *Addit. Manuf.* **2020**, *35*, No. 101177.
- (19) Bennett, J. Measuring UV Curing Parameters of Commercial Photopolymers Used in Additive Manufacturing. *Addit. Manuf.* **2017**, *18*, 203–212.
- (20) Martin, B.; Puentes, J.; Wruck, L.; Osswald, T. A. Degree of Cure of Epoxy/Acrylic Photopolymers: Characterization with Raman Spectroscopy and a Modified Phenomenological Model. *Polym. Eng. Sci.* **2018**, *58* (2), 228–237.
- (21) Choong, Y. Y. C.; Maleksaeedi, S.; Eng, H.; Yu, S.; Wei, J.; Su, P.-C. High Speed 4D Printing of Shape Memory Polymers with Nanosilica. *Appl. Mater. Today* **2020**, *18*, No. 100515.
- (22) Robakowska, M.; Gierz, Ł.; Mayer, P.; Szcześniak, K.; Marcinkowska, A.; Lewandowska, A.; Gajewski, P. Influence of the Addition of Sialon and Aluminum Nitride Fillers on the Photocuring Process of Polymer Coatings. *Coatings* **2022**, *12* (10), 1389.
- (23) Schlotthauer, T.; Nolan, D.; Middendorf, P. Influence of Short Carbon and Glass Fibers on the Curing Behavior and Accuracy of Photopolymers Used in Stereolithography. *Addit. Manuf.* **2021**, 42, No. 102005.
- (24) Xu, Y.; Ding, Z.; Zhu, H.; Zhang, Y.; Knopf, S.; Xiao, P.; Lalevée, J. Preparation of Iron Filler-Based Photocomposites and Application in 3D Printing. *Macromol. Mater. Eng.* **2021**, *306* (3), No. 2000720.
- (25) Xing, H.; Zou, B.; Liu, X.; Wang, X.; Huang, C.; Hu, Y. Fabrication Strategy of Complicated Al2O3-Si3N4 Functionally Graded Materials by Stereolithography 3D Printing. *J. Eur. Ceram. Soc.* **2020**, 40 (15), 5797–5809.
- (26) Zhao, T.; Yu, R.; Li, X.; Zhang, Y.; Yang, X.; Zhao, X.; Huang, W. A Comparative Study on 3D Printed Silicone-Epoxy/Acrylate Hybrid Polymers via Pure Photopolymerization and Dual-Curing Mechanisms. *J. Mater. Sci.* **2019**, *54* (6), 5101–5111.
- (27) Jiao, T.; Lin, Y.; Liu, Y.; Liu, J.; Lu, G. Effect of Modified Calcium Sulphate Whiskers on Free-Radical/Cationic Hybrid Photopolymers for 3D Printing. *Mater. Res. Express* **2020**, 7 (1), No. 015334
- (28) Zhao, J.; Li, Q.; Jin, F.; He, N. Digital Light Processing 3D Printing Kevlar Composites Based on Dual Curing Resin. *Addit. Manuf.* **2021**, *41*, No. 101962.
- (29) Xu, Y.; Jambou, C.; Sun, K.; Lalevée, J.; Simon-Masseron, A.; Xiao, P. Effect of Zeolite Fillers on the Photopolymerization Kinetics for Photocomposites and Lithography. *ACS Appl. Polym. Mater.* **2019**, 1 (11), 2854–2861.
- (30) Wu, J.; Zhao, Z.; Kuang, X.; Hamel, C. M.; Fang, D.; Qi, H. J. Reversible Shape Change Structures by Grayscale Pattern 4D Printing. *Multifunct. Mater.* **2018**, *1* (1), No. 015002.
- (31) Wu, K. C.; Halloran, J. W. Photopolymerization Monitoring of Ceramic Stereolithography Resins by FTIR Methods. *J. Mater. Sci.* **2005**, *40* (1), 71–76.
- (32) Lyon, R. E.; Chike, K. E.; Angel, S. M. In Situ Cure Monitoring of Epoxy Resins Using Fiber-Optic Raman Spectroscopy. *J. Appl. Polym. Sci.* **1994**, 53 (13), 1805–1812.
- (33) Jeng, J.-Y.; Wong, Y. S.; Ho, C. T. Curing Characteristics of the Photopolymer Used in the Solid Laser-Diode Plotter RP System. *Int. J. Adv. Manuf Technol.* **2001**, *17* (7), 535–542.
- (34) McClain, M. S.; Afriat, A.; Rhoads, J. F.; Gunduz, I. E.; Son, S. F. Development and Characterization of a Photopolymeric Binder for Additively Manufactured Composite Solid Propellant Using Vibration

- Assisted Printing. Propellants, Explos., Pyrotech. 2020, 45 (6), 853-863.
- (35) Dawan, F.; Ekuase, O. A.; Mensah, P. F. In *Thermo-Mechanical Characterization of a Hybrid Reinforced Photopolymer Composite Via DLP 3D Printing*, American Society for Composites 35th Annual Technical (Virtual) Conference 2020, 2020.
- (36) Yang, Z.; Peng, S.; Wang, Z.; Miao, J.-T.; Zheng, L.; Wu, L.; Weng, Z. UV-Curable, Low-Viscosity Resin with a High Silica Filler Content for Preparing Ultrastiff, 3D-Printed Molds. ACS Appl. Polym. Mater. 2022, 4 (4), 2636–2647.
- (37) Gao, Y.; Yang, W.; Hu, R.; Zhou, J.; Zhang, Y. Validation of CL-20-Based Propellant Formulations for Photopolymerization 3D Printing. *Propellants, Explos., Pyrotech.* **2021**, 46 (12), 1844–1848.
- (38) Gaidukovs, S.; Medvids, A.; Onufrijevs, P.; Grase, L. UV-Light-Induced Curing of Branched Epoxy Novolac Resin for Coatings. *Express Polym. Lett.* **2018**, *12*, 918–929.
- (39) McKeen, L. W. Fluorinated Coatings and Finishes Handbook: The Definitive User's Guide; William Andrew, 2015; p 294.
- (40) Anycubic Resin User Manual & MSDS; ANYCUBIC 3D Printing, 2023. https://www.anycubic.com/pages/resin-user-manual.
- (41) Spencer Tipping. Novum Glass, 2023. https://www.novumglass.com/.
- (42) Rau, D. A.; Reynolds, J. P.; Bryant, J. S.; Bortner, M. J.; Williams, C. B. A Rheological Approach for Measuring Cure Depth of Filled and Unfilled Photopolymers at Additive Manufacturing Relevant Length Scales. *Addit. Manuf.* **2022**, *60*, No. 103207.
- (43) Swinehart, D. F. The Beer-Lambert Law. J. Chem. Educ. 1962, 39 (7), 333.
- (44) Hofstetter, C.; Orman, S.; Baudis, S.; Stampfl, J. Combining Cure Depth and Cure Degree, a New Way to Fully Characterize Novel Photopolymers. *Addit. Manuf.* **2018**, 24, 166–172.
- (45) Sampson, K. L.; Deore, B.; Go, A.; Nayak, M. A.; Orth, A.; Gallerneault, M.; Malenfant, P. R. L.; Paquet, C. Multimaterial Vat Polymerization Additive Manufacturing. *ACS Appl. Polym. Mater.* **2021**, *3* (9), 4304–4324.
- (46) Jacobs, P. F. In Fundamentals of Stereolithography, 1992 International Solid Freeform Fabrication Symposium, 1992.
- (47) Bradley, M. Curve Fitting in Raman and IR Spectroscopy: Basic Theory of Line Shapes and Applications; Thermo Fisher Scientific: Madison, USA, 2007.
- (48) Mao, Q.; Bian, L.; Huang, M. Study of the Visible Light Curing of Vinyl Ester Resins Using in Situ Raman Spectroscopy. *J. Polym. Res.* **2011**, *18* (6), 1751–1756.
- (49) ISO 25178-2:2021(En). Geometrical Product Specifications (GPS)—Surface Texture: Areal—Part 2: Terms, Definitions and Surface Texture Parameters, 2022. https://www.iso.org/obp/ui/#iso:std:iso:25178:-2:ed-2:v1:en.
- (50) Hulst, H. C.; van de Hulst, H. C. Light Scattering by Small Particles; Courier Corporation, 1981; p 11.
- (51) Jiang, F.; Drummer, D. Curing Kinetic Analysis of Acrylate Photopolymer for Additive Manufacturing by Photo-DSC. *Polymers* **2020**, *12* (5), 1080.
- (52) Caputo, F.; Clogston, J.; Calzolai, L.; Rösslein, M.; Prina-Mello, A. Measuring Particle Size Distribution of Nanoparticle Enabled Medicinal Products, the Joint View of EUNCL and NCI-NCL. A Step by Step Approach Combining Orthogonal Measurements with Increasing Complexity. *J. Controlled Release* **2019**, 299, 31–43.